---

**Article:**
Noble, C., Smulders, N., Green, N.H. orcid.org/0000-0001-5413-0642 et al. (5 more authors) (2016) Creating a model of diseased artery damage and failure from healthy porcine aorta. Journal of the Mechanical Behavior of Biomedical Materials, 60. pp. 378-393. ISSN 1751-6161

https://doi.org/10.1016/j.jmbbm.2016.02.018

---

# Creating a model of diseased artery damage and failure from healthy porcine aorta

Christopher Noble[a,*], Nicole Smulders[b], Nicola H. Green[c], Roger Lewis[d], Matt J. Carré[d], Steve E. Franklin[b], Sheila MacNeil[c], Zeike A. Taylor[a]

[a] *CISTIB, Centre for Computational Imaging and Simulation Technologies in Biomedicine, INSIGNEO Institute for in silico Medicine,Department of Mechanical Engineering, The University of Sheffield, Sheffield, UK*
[b] *Philips Research, Eindhoven, The Netherlands*
[c] *Department of Materials Science and Engineering, The Kroto Research Institute, North Campus, University of Sheffield, Broad Lane, Sheffield, UK*
[d] *Department of Mechanical Engineering, The University of Sheffield, Sheffield, UK*

**Abstract**

Large quantities of diseased tissue are required in the research and development of new generations of medical devices, for example for use in physical testing. However, these are difficult to obtain. In contrast, porcine arteries are readily available as they are regarded as waste. Therefore, reliable means of creating from porcine tissue physical models of diseased human tissue that emulate well the associated mechanical changes would be valuable. To this end, we studied the effect on mechanical response of treating porcine thoracic aorta with collagenase, elastase and glutaraldehyde. The alterations in mechanical and failure properties were assessed via uniaxial tension testing. A constitutive model composed of the Gasser-Ogden-Holzapfel model, for elastic response, and a continuum damage model, for the failure, was also employed to provide a further basis for comparison [1, 2]. For the concentrations used here it was found that: collagenase treated samples showed decreased fracture stress in the axial direction only; elastase treated samples showed increased fracture stress in the circumferential direction only; and glutaraldehyde samples showed no change in either direction. With respect to the proposed constitutive model, both collagenase and elastase had a strong effect on the fibre-related terms. The model more closely captured the tissue response in the circumferential direction, due to the smoother and sharper transition from damage initiation to complete failure in this direction. Finally, comparison of the results with those of tensile tests on diseased tissues suggests these treatments indeed provide a basis for creation of physical models of diseased arteries.

*Keywords:* Diseased tissue model, Porcine aorta, Collagenase, Elastase, Glutaraldehyde, Uniaxial tension

## Nomenclature

| | |
|---|---|
| 20hC | Control samples incubated for 20 hours |
| $\Psi$ | Strain energy density function |
| $\mathbf{C}$ | Right Cauchy-Green deformation tensor |
| $\mathbf{I}$ | 2nd order identity tensor |
| $\mathbf{H}_i$ | General structural tensor for fibre family $i$ |
| $E_i$ | Strain in the direction of mean fibre orientation for fibre family $i$ |
| $\lambda_1, \lambda_2, \lambda_3$ | Principal stretches |
| $\theta$ | Mean collagen fibre angle |
| $\mathbf{a}_i$ | Unit vector describing mean collagen fibre orientation for fibre family $i$ |

*Corresponding author
*Email address:* mta08cn@sheffield.ac.uk (Christopher Noble)

| | |
|---|---|
| $\kappa$ | Statistical parameter describing the degree of collagen fibre dispersion |
| $\mu$ | Shear modulus |
| $k_1$ | Stress like parameter within GOH model |
| $k_2$ | GOH model fibre material parameter |
| $\sigma_1, \sigma_2, \sigma_3$ | Principal Cauchy stresses |
| $p$ | Lagrange multiplier |
| $D^k$ | Reduction factor |
| $\Xi_t^k$ | Damage criterion |
| $\Xi_{min}^k$ | Damage initiation parameter |
| $\Xi_{max}^k$ | Damage completion parameter |
| $\beta^k$ | Damage profile control parameter |
| $f$ | Measured reaction force |
| $T$ | Sample thickness |
| $W$ | Sample width |
| $\mathbf{x}$ | Vector of model parameters |
| $w_1, w_2$ | Weighting parameters |
| $\sigma_1^{\exp}$ | Experimentally measured first principal Cauchy stress |
| $\sigma_1^{mod}$ | Model-predicted first principal Cauchy stress |

## 1. Introduction

Cardiovascular disease accounted for almost 3 in every 10 deaths in the United Kingdom in 2014 [3], requiring huge investments of time, money and other resources to treat. The creation of a new generation of medical devices (such as endovascular catheters and stents) to combat this requires significant *in vitro* research with arterial tissue. Ideally, diseased tissue, properly reflecting the *in vivo* conditions experienced by these devices, should be used. However, obtaining diseased human tissue in sufficient quantities is difficult (both practically and ethically) and costly. By contrast, porcine arteries are considered waste tissue by abattoirs and so are readily available. But, their mechanical response differs due to the effects of disease and ageing and the differing properties between human and porcine tissue [4, 5]. Thus the creation of a human diseased tissue model from healthy porcine aorta potentially would ameliorate the cost and complexity of medical device design.

The variation of mechanical properties between healthy porcine tissue and diseased human tissue is a result of differences in the structure, concentrations and properties of the arterial wall constituents. Mammalian arteries are multi-layered structures composed of various fibre and cellular constituents, whose alignment and composition vary depending on the pressure in the vessel and the proximity to the heart [6]. Regardless, all have some common features: an intimal layer made up of endothelial cells and the elastic lamina; a medial layer, composed mostly of elastin fibres but also with smooth muscle cells and collagen fibres; and an adventitial layer containing primarily collagen fibres [7].

Regional variations in the structural arrangement of these components produces similar variations in the regional anisotropic behaviour. Disease and ageing, however, alter the respective compositions, leading to often undesirable changes in function. Ageing has been shown to cause a loss of medial elastin followed by an increase in the stiffer collagen fibres, further stiffened by additional cross-linking, to compensate [8, 9, 10, 11]. This results in the elastin-collagen interaction altering and the stiffer collagen fibres being recruited at smaller deformations, leading to an observed stiffening of the arterial wall. Whilst in aneurysm formation, the characteristic ballooning is also widely attributed to loss of elastin and a resulting loss of stiffness in the artery [12, 13]. In atherosclerosis, changes in elastin and collagen structure again weaken the medial and intimal layers [14, 15, 16]. Genetic diseases such as Marfan syndrome can also have large effects on collagen and elastin fibres leading to greatly reduced stiffness and toughness in blood vessel walls [17]. These changes are often complex and multifaceted. Correspondingly, alterations such as the loss of elastin may increase or decrease stiffness depending on a variety of co-factors.

Previous work aimed at understanding these mechanisms by utilising enzymatic digestion to emulate diseased arterial properties *in vitro,* and at understanding and characterising the changes in material response under loading via mechanical testing. Both uniaxial and biaxial testing have been performed on tissue treated with collagenase and elastase to understand the alteration in material behaviour [18, 19, 20]. In addition, inflation tests have been performed to enhance physiological relevance [21, 22, 23, 24]. However, only one previous study has been identified that investigated the failure response of these tissues after treatment, of which there is a necessity as the progression of most arterial diseases will ultimately result in failure of the tissue in some form [25]. Furthermore, many treatments for such disease will themselves damage the tissues, on occasion leading to catastrophic tissue failure, e.g. weakened atherosclerotic blood vessel wall rupturing during stent placement.

In this paper, the effects on artery mechanical response of disease-mimicking enzymatic digestion are investigated. Particular attention is paid to the effect on damage and failure behaviour, when tissue specimens are stretched beyond physiological (and elastic) limits. As in the work mentioned previously, enzymatic digestion was applied to porcine aortic media samples, to degrade the constituent proteins. Low concentration glutaraldehyde treatment was also utilised, as an alternative method to mimic cross-linking and stiffening seen in processes like glycation [26, 27]. Treated tissue was then stretched to failure in both the vessel axial and circumferential directions. Constitutive models were then employed to allow description and comparison of the overall tissue response under loading. This allowed the gradual changes in the mechanical response to be related to the structural alterations associated with the different treatment types. The well-known Gasser-Ogden-Holzapfel (GOH) model was utilised for the elastic component of the tissue response (prior to damage). This model compromises an isotropic neo-Hookean term, accounting for the elastin fibres and ground substance, and an exponential term for each of the two collagen fibre families [2]. The damage and failure behaviour were captured using the continuum damage model (CDM) described in [1], which has previously been shown to capture well the failure behaviour of arterial tissue when combined with the GOH model [28].

## 2. Methods

### *2.1. Mechanical Testing*

#### *2.1.1. Sample Preparation*

Porcine aorta was chosen as the experimental model due to (i) its availability, allowing many tests to be performed, and (ii) its thickness, allowing the media and intima, the layers most affected by disease processes, to be easily tested in isolation. Control tissue was tested within 24 hours of the slaughter of the animal and treated tissue within 48 hours, the latter owing to the additional incubation time associated with the treatments. All tissue was stored in a refrigerator when not undergoing treatment.

The aorta was initially cut into 40×15 mm pieces aligned in axial and circumferential directions and the adventitial layer was carefully removed. The remaining tissue was carefully cut into a dog bone shape with approximately 5 mm gauge width and 10 mm length and stored in solution.

All non-control samples were then treated with their respective solutions as described in table 1. All treatments were diluted in saline solution with antibiotics (Penicillin and Streptomycin) and fungicide to prevent growth of micro-organisms. To ensure the accompanying incubation process had no effect on sample mechanical properties, an additional group of controls were incubated for 20 hours and tested. Following treatment, all samples were washed thoroughly with saline solution to remove trace elements of chemical and enzymes.

#### *2.1.2. Test Protocol*

Specimens were prepared for tensile testing by carefully adhering two pairs of small black markers to the gauge region, using tweezers and super-glue. These allowed measurement, via optical means, of the stretches in the first and second principal directions [29]. Representative sample geometry and marker placement is shown in figure 1. Test specimens were placed back in saline solution for around 5 seconds to moisten them

after placing the markers, and placed in grips mounted to a Tinius Olsen 5 kN tensile machine. The grips had serrated edges which prevented slippage; thus, the addition of sand paper was not necessary for this study. In some previous studies, samples were placed in a saline bath at 37°C to improve the physiological relevance of the test conditions. However, since distortion by refraction could then reduce the accuracy of the marker position recording, this was not done here [30]. Preconditioning was performed by applying 10 displacement loading cycles of 15 mm at 0.1 Hz with a final, 11th, loading cycle constituting the recorded experiment. The test was filmed using a Fujifilm Finepix Z90 digital camera. Accuracy and effects such as image distortion by the lens were investigated prior to use, and found to be insignificant. TrackMate plug-in within Fiji software[1] was utilised with the recording to register and track the paired markers to ascertain stretch in each principal direction. The recording equipment was also utilised with Fiji to measure the tissue initial width and thickness, by photographing the unloaded tissue with a ruler adjacent for scale.

### *2.2. Constitutive Modelling*

Motivated by the nonlinearity and anisotropy of arterial walls [31, 32], we have utilised the GOH model to describe the elastic behaviour [2]. This has been used frequently to capture the response of arterial walls in uniaxial tension [33, 34, 20]. Weakening of the material, as it is deformed beyond its elastic range, and ultimate failure is incorporated into the model by means of a continuum damage model (CDM) [1]. The CDM components scales the stress according to the level of damage the tissue has undergone. It becomes active only after damage initiation conditions have been met.

#### *2.2.1. Elastic Response*

The strain energy function $\Psi$ of the GOH model comprises an isotropic Neo-Hookean term $\Psi^m$, accounting for elastin fibres and ground matrix, and anisotropic exponential terms $\Psi^f$, for each of two families of collagen fibres:

$$\Psi(\mathbf{C}, \mathbf{H}_i) = \Psi^m(\mathbf{C}) + \sum_{i=1,2} \Psi_i^f(\mathbf{C}, \mathbf{H}_i(\mathbf{a}_i, \kappa)), \tag{1}$$

with

$$\Psi^m(\mathbf{C}) = \frac{\mu}{2}(\lambda_1^2 + \lambda_2^2 + \lambda_3^2 - 3) \tag{2}$$

and

$$\Psi_i^f(\mathbf{C}, \mathbf{H}_i) = \frac{k_1}{2k_2}[\exp(k_2 E_i^2) - 1],\ i = 1, 2 \tag{3}$$

where

$$E_i = \mathbf{H}_i : \mathbf{C} - 1, \quad \mathbf{H}_i = \kappa\mathbf{I} + (1 - 3\kappa)(\mathbf{a}_i \otimes \mathbf{a}_i). \tag{4}$$

The principal stretches are given as $\lambda_1$, $\lambda_2$ and $\lambda_3$, with directions of the first two indicated in figure 1, and the mean collagen fibre direction $\theta$, figure 2, in the reference configuration is characterised by unit vectors $\mathbf{a}_i$. Here $\mathbf{a}_1 = [\sin(\theta)\ \cos(\theta)\ 0]$ and $\mathbf{a}_2 = [-\sin(\theta)\ \cos(\theta)\ 0]$ when $\lambda_1$ is in the axial direction and $\mathbf{a}_1 = [\cos(\theta)\ \sin(\theta)\ 0]$ and $\mathbf{a}_2 = [-\cos(\theta)\ \sin(\theta)\ 0]$ when $\lambda_1$ is in the circumferential direction.

The degree of fibre dispersion is captured by a statistical parameter $\kappa \in [0, \frac{1}{3}]$, where $\kappa = 0$ denotes complete alignment of fibres, while $\kappa = \frac{1}{3}$ implies full dispersion, resulting in isotropy. Additional parameters are $\mu$, the shear modulus, $k_1$, a stress-like parameter and $k_2$, a dimensionless parameter. The second order tensors $\mathbf{C}$ and $\mathbf{I}$ are the right Cauchy-Green deformation tensor and the identity, tensor respectively.

[1] **http://fiji.sc/TrackMate**

Additionally, the second order tensor $\mathbf{H}_i(\mathbf{a}_i, \kappa)$ is a general structural tensor for fibre family $i$. Finally the scalar parameter $E_i$ characterises the strain in the direction of the mean fibre orientation for the $i^{th}$ fibre family.

A fundamental hypothesis of the model is that the collagen fibres do not provide resistance to compressive stresses and simply buckle under compressive loading. This is represented within the model by allowing the $(1-3\kappa)(\mathbf{a}_i \otimes \mathbf{a}_i)$ component of $\mathbf{H}_i$ to be active only when $\mathbf{C} : (\mathbf{a}_i \otimes \mathbf{a}_i) > 1$.

The principal Cauchy stresses may be computed from the strain energy function according to [35]:

$$\sigma_a = -p + \lambda_a \frac{\partial \Psi}{\partial \lambda_a}, \quad a = 1, 2, 3 \tag{5}$$

where $p$ is a Lagrange multiplier with the physical interpretation of the hydrostatic pressure. Using standard assumptions and arguments, the first principal stress can be shown to be:

$$\sigma_1(\lambda_1, \lambda_2, \mathbf{a}_1, \mathbf{a}_2) = \sigma_1^m(\lambda_1, \lambda_2) + \sum_{i=1,2} \sigma_{i1}^f(\lambda_1, \lambda_2, \mathbf{a}_1, \mathbf{a}_2), \tag{6}$$

where the individual terms, $\sigma_1^m$ and $\sigma_{i1}^f$, are too long to reproduce here. Further information on the assumptions and derivation can be found in appendix A.

*2.2.2. Damage Model*

The CDM is incorporated by augmenting (1) as:

$$\Psi(\mathbf{C}, \mathbf{H}_i, D^m, D^f) = (1 - D^m)\Psi^m(\mathbf{C}) + (1 - D^f) \sum_{i=1,2} \Psi_i^f(\mathbf{C}, \mathbf{H}_i(\mathbf{a}_i, \kappa)), \tag{7}$$

Here $(1 - D^m)$ and $(1 - D^f)$ are known as the reduction factors, with $D^m \in [0, 1]$ and $D^f \in [0, 1]$ being normalised scalars for the matrix and fibre families, respectively, referred to hereafter as damage multipliers [36]. Using (7) with standard constitutive continuum mechanical arguments, (6) becomes for the damage case:

$$\sigma_1 = (1 - D^m)\sigma_1^m + (1 - D^f) \sum_{i=1,2} \sigma_{i1}^f \tag{8}$$

Evolution of the damage multipliers $D^m$ and $D^f$ are characterised by their respective damage criterion $\Xi_t^m$ and $\Xi_t^f$:

$$\Xi_t^m = \max_{s \in (-\infty, t)} \sqrt{2\Psi^m(\mathbf{C}(s))} \tag{9}$$

$$\Xi_t^f = \max_{s \in (-\infty, t)} \sqrt{2 \sum_{i=1,2} \Psi_i^f(\mathbf{C}(s))} \tag{10}$$

where $\mathbf{C}(s)$ is the right Cauchy-Green tensor at time $s$.

The damage evolution is characterised by (11) with $\xi = (\Xi_t^k - \Xi_{\min}^k)/(\Xi_{\max}^k - \Xi_{\min}^k)$, for $k = m, f$ [37]:

$$D^k(\Xi_t^k) = \begin{cases} 0 & if\ \Xi_t^k < \Xi_{\min}^k \\ \xi^2[1 - \beta^k(\xi^2 - 1)] & if\ \Xi_{\min}^k \leq \Xi_t^k \leq \Xi_{\max}^k \\ 1 & if\ \Xi_t^k > \Xi_{\max}^k \end{cases} \tag{11}$$

$\Xi_{\min}^k$ and $\Xi_{\max}^k$ denote critical values of the damage criteria at which, respectively, damage is initiated and completed. $\beta^k \in [-1.0, 1.0]$ is a dimensionless variable that controls the damage profile. The behaviour encapsulated in (11) is depicted in figure 3.

*2.2.3. Curve Fitting*

As described in [33], for the uniaxial tension test configuration, the first principal stress may be computed from:

$$\sigma_1 = \frac{f}{TW}\lambda_1 \tag{12}$$

Here $f$ is the measured reaction force, $W$ and $T$ are the initial width and thickness, respectively, and $\lambda_1$ is the uniaxial stretch. Fitting of the GOH and CDM parameters to the experimental data was performed using the optimisation toolbox within MATLAB. The fitting procedure was formulated as the optimisation problem described in (13):

$$\mathbf{x} = \underset{\mathbf{x}}{\arg\min} \left\{ w_1 ||\sigma_1^{exp} - \sigma_1^{mod}||_2^{axial} + w_2 ||\sigma_1^{exp} - \sigma_1^{mod}||_2^{circ} \right\} \tag{13}$$

Here $\mathbf{x}$ is a vector of model parameters, $\sigma_1^{\exp}$ are experimentally measured first principal Cauchy stresses (vector of values, measured over the course of the experiment), computed using (12), and $\sigma_1^{\mathrm{mod}}$ are the corresponding model-predicted stresses, computed using (8). $w_1$ and $w_2$, are weighting parameters, manually tuned to achieve best fit, $||\cdot||_2$ denotes the 2-norm and "axial" and "circ" pertain to data derived from axial and circumferential specimens, respectively.

To improve optimisation time and robustness, GOH model parameters were found separately from damage parameters. This was done by fitting to the experimental data up to the estimated point of damage initiation, identified through inspection of experimental data. CDM parameters were then optimised over the whole data set with the previously found GOH parameters.

To reduce the computational cost and robustness of the optimisation procedure, several parameters were either assigned literature values or deduced by inspection. $\kappa$ was set to 0.046 in accord with Shriefl et al. [38]. The shear modulus $\mu$ was fixed at 3 kPa (based on initial tests and values found in previous studies [33]), as initial tests revealed that altering it had little effect on the overall behaviour at the large stretches seen here, where the exponential fibre terms dominate. Correspondingly, the matrix component of the CDM was also omitted thereafter. Fibre damage parameters $\Xi^f_{\min}$ and $\Xi^f_{\max}$ were estimated according to: $\Xi^f_{\min} = \sqrt{2\sum_{i=1,2}\Psi^f_i(\lambda_1^I)}$ and $\Xi^f_{\max} = \sqrt{2\sum_{i=1,2}\Psi^f_i(\lambda_1^F)}$, where $\lambda_1^I$ and $\lambda_1^F$ are stretches at which damage initiated and at which complete failure of the specimens occurred, respectively. These stretches were estimated by direct inspection of the experimental curves. Therefore, the remaining constitutive parameters estimated during the fitting procedures are as summarised in table 2.

There are multiple ways in which model parameter fitting to the experimental data can be approached. A possible solution is to fit to each data set independently, then average the parameters for the constitutive model to give the overall behaviour in each direction. This method is computationally costly and as Roberson and Cook have shown, averaged constitutive parameters are not guaranteed to represent average behaviour [39]. In this work, therefore, the model was fit to averaged curves only, and to both directions simultaneously (as described by (13)). Thus material parameters were produced that encapsulate the material behaviour more closely.

A particle swarm optimisation procedure was utilised [40]. This global optimisation method operates by selecting multiple starting points, known as particles. This is advantageous as it reduces optimum solution dependence on the starting parameters, which is otherwise a common occurrence when fitting hyperelastic constitutive models [41]. The movement of each particle is governed by simple mathematical formulae describing the particle's position and velocity. Each particle's movement is influenced by its local best known position , but also by the progress of other particles, as they find better positions elsewhere in the search space. This moves the swarm to the best solution whilst not being reliant on the gradient of the search space, unlike the commonly used nonlinear least squares algorithm. This allows it to find an approximate minimum despite the irregular search space that is present here. Once the particle swarm optimisation has concluded, a least squares optimisation algorithm is called, beginning at the best known location from the swarm, to

further refine the solution. Finally, upper and lower bounds were imposed on the model parameters to limit the search space of the optimiser and ensure physical plausibility.

## 3. Results

### *3.1. Mechanical Tests*

The observed stress responses up to fracture of the tested specimens are shown in figures 4 and 5. Overall large variation in results are present, however statistically significant differences, assessed via the students unpaired $t$-test, in fracture behaviour can be seen (table 3). A summary of salient features of these responses for the various categories of specimens follows below:

*Circumferential versus axial specimens.* Circumferential specimens displayed higher fracture stress ($p<0.05$ for all samples) while axial specimens have higher fracture stretches ($p<0.05$ for all samples). An additional trend seen in both control samples and glutaraldehyde samples is the fragmented response under loading in the axial direction: the curves show some flattening and dips associated with minor localised failure before final fracture.

*Control versus 20 hour control (20hC) specimens.* Samples from both groups show similar behaviour with minor changes in fracture stress and stretch that are not significantly different ($p \not< 0.05$).

*Control versus collagenase specimens.* Collagenase circumferential results are more scattered, with less well defined peaks and some evidence of localised failure before the final fracture. Furthermore, the stretch at which fracture occurs is greater ($p<0.05$), the curves showing an overall shift to the right. However, the fracture stress is only marginally lower (no statistical significance). In the axial direction, the collagenase specimens are far less stiff, with a lower fracture stress ($p<0.05$) and higher fracture stretch ($p<0.05$).

*Control versus elastase specimens.* Elastase treated samples show an increase in fracture stress and stretch in both directions. However, in the axial direction, only the stretch is significantly different ($p<0.05$), whilst in the circumferential direction both the fracture stress and stretch are significant ($p<0.05$). The highest fracture stretches (approximately 2.8) across all treatments can be seen here in the axial direction.

*Control versus glutaraldehyde specimens.* Glutaraldehyde samples in the circumferential direction show a higher spread in fracture stress, but similar fracture stretches, with differences less stark than in the collagenase treated samples. While in the axial direction, the fracture stress and stretch are similar to the control samples, but the already fragmented fracture behaviour is now further exaggerated, with damage initiating earlier.

### *3.2. Curve Fitting*

The resulting GOH parameters are given in table 4a. Glutaraldehyde treated samples yielded the highest $k_1$, with collagenase values significantly lower than all others. All treatments resulted in substantially lower $k_2$ values than for the controls, with elastase specimens yielding the lowest. Finally the collagen fibre angle is lowest for collagenase but highest for elastase samples, though the difference is small: $< 4^{\circ}$.

The damage parameters were also sought from the averaged curves, but $\Xi^f_{\text{min}}$ and $\Xi^f_{\text{max}}$ were found to be different in the axial and circumferential directions (table 4b). Additionally trial experiments showed that fitting $\beta^f$ to both directions simultaneously produced poor fits (discussed further in section 4.2.1) and so the damage parameters were fit to each direction separately.

The damage parameters so obtained are given in table 4b. For $\Xi^f_{\text{min}}$ and $\Xi^f_{\text{max}}$ in the axial direction, glutaraldehyde samples produced the highest spread (highest $\Xi^f_{\text{max}}$ but third lowest $\Xi^f_{\text{min}}$). Collagenase shows the lowest spread with the lowest $\Xi^f_{\text{min}}$ and lowest $\Xi^f_{\text{max}}$. The optimised value of $\beta^f$ is highest for control samples, but varies greatly, with collagenase samples showing the lowest.

In the circumferential direction, collagenase produced the highest spread between $\Xi^f_{\text{min}}$ and $\Xi^f_{\text{max}}$, with the lowest $\Xi^f_{\text{min}}$ and second highest $\Xi^f_{\text{max}}$, whilst the control samples produced the lowest spread. Interestingly, $\Xi^f_{\text{min}}$ for elastase is greater than $\Xi^f_{\text{max}}$ for all other samples. $\beta^f$ is lowest for glutaraldehyde and highest for collagenase. The collagenase experimental data and the fitted curve show the slowest progression to failure, which coincides with the highest spread between damage terms, $\Xi^f_{\text{min}}$ and $\Xi^f_{\text{max}}$.

The overall quality of the fits is assessed by the coefficient of determination $r^2$ measure (table 4c). The fits in the circumferential direction were all of high quality, with $r^2 \geq 0.97$, but especially in the control samples where, in figure 6, the experimental and fitted data are almost indistinguishable. Poorer fits were obtained for axial data, with control data yielding the weakest fit ($r^2 = 0.850$). The resulting model-predicted curves are shown in figure 6.

Comparing between directions it can be seen that the spread of the damage terms is overall higher for the axial direction. This is reflected in the curves as a more gradual progression to failure for the axial data, whereas the circumferential data show a sharper progression (figure 6).

## 4. Discussion

### *4.1. Mechanical Tests and Effects of Digestion*

Results from uniaxial tests generally coincide with the anisotropic behaviour seen elsewhere [42, 43, 31]. The stiffer behaviour in the circumferential direction is greater because of greater alignment with the stiffer collagen fibres. This in turn leads to a greater fracture stress in the circumferential direction. The difference in fracture stretch is likely due to the high stress in the circumferential direction, such that once the tensile strength of collagen has been reached the elastin and surrounding matrix also breaks. Whereas the stress in the axial direction is far lower, the increasing slope of the curves suggests that collagen is still the major contributor to the behaviour at high stretch. The alignment of fibres could also explain the fragmented fracture behaviour seen in the axial direction, as the drops could be associated with fibres families pulling apart, rather than breaking outright .

The magnitude of the stress in the control samples is higher here than reported in other publications [44]. However, a possible explanation is that preconditioning was performed up to 15 mm and samples were extended further than this when stretched to failure. Thus the region between 15 mm displacement and failure will show greater time-dependent behaviour and it has been previously shown that loading rate affects the failure stress and stretch [45, 46, 47]. Nevertheless, all tests were performed under the same conditions and as such all comparisons between treatment types remain valid.

The variation in the curve profiles and fracture behaviour may be attributed to structural variations between individual animals and anatomical locations, and also to the difference in thickness of the samples, affecting the extent of digestion. Despite the samples being incubated for 20 hours, thicker samples will require longer for the enzymes to permeate to the centre and thus thinner samples would be expected to be more digested [48].

#### *4.1.1. Collagenase treatment*

The effect of collagenase digestion on wall compliance varies in the literature. Dobrin and coworkers found that there was no change in axial compliance with collagenase treatment, contradicting the results of this study [49, 50]. However Gundiah et al. found collagenase treatment affected wall compliance in both directions, which supports the findings here [18]. The differences in behaviour in this study are most pronounced in the axial direction, with both the fracture stress and stretch being significantly different, whilst only the stretch is significantly different in the circumferential direction. This is an unexpected result because it has been shown the collagen fibres in the intima and media are more aligned with the circumferential direction (albeit marginally so in the intima). Differences in fracture properties would therefore be *most* expected in this direction [38].

It is perhaps explained by the relationship between elastin and collagen in the arterial wall: detachment of collagen from elastin fibres in the axial direction may lead to collagen fibres not being recruited and thus the flat, highly extensible behaviour in the axial direction. The digestion may have been insufficient to alter the fracture stress in the circumferential direction, but enough to cause collagen to detach from the elastin fibres in the axial direction. Many of the curve profiles in the circumferential direction have lost the smooth behaviour seen in the control study, and instead show a disrupted shape which may reflect disruption of the collagen fibre network.

*4.1.2. Elastase Treatment*

The behaviour resulting from elastase treatment is mostly different from that reported in other publications, where elastin digestion instead is reported to result in a loss of compliance and an immediate collagen-related stiffening [51, 34]. However, Chow et al. have shown that partial digestion of elastin tends to increase the compliance of the tissue, which would support the increased fracture stretch [52]. They describe the increased compliance region followed by a sudden stiffening as the "extensible but stiff" region, which shows varying initial compliance depending on the amount of elastin degradation and which is also supported by other studies [31, 53]. However, to our knowledge, no study examined the tensile behaviour of elastase treated artery up to failure, and so speculation as to the causes of this behaviour is difficult. However, it is interesting to note the behaviour of the average elastase treated sample in the circumferential direction when compared to that of the 20hC and control samples (figure 7). Despite a slight shift to the right and an increase in fracture stress/stretch, the elastase curve follows a similar profile to the two control curves. A possible reason is that this is an innate response of the tissue to elastin loss/damage. Loss of elastin leads to the alteration of collagen and elastin interconnectivity such that collagen bears more of the load and the fracture stress increases. This acts to shield the remaining elastin from further damage whilst further protecting the vessel from rupture.

*4.1.3. Glutaraldehyde Treatment*

The ability of glutaraldehyde to cross-link and stiffen proteins has been exploited for various applications and is widely used for fixing biological samples for histological examination [54, 55, 56]. This capability has been suggested elsewhere for altering mechanical properties of vascular grafts to match those of the host [57, 58]. These studies found an increase in stiffness and tensile strength with treatment, which was not evident here despite treatment concentrations and durations being similar. Despite this, an increase in fragmented behaviour in individual curves compared to the control samples in the axial direction can be observed. It is possible that at this concentration, the treatment is most effective on cross links between existing fibre bundles, causing existing links to become more brittle, and easing the separation from one another of fibre bundles.

*4.2. Parameter Fitting and Effects of Digestion*

*4.2.1. Quality and Reliability of the Fits*

Comparison of the quality of the curve fits in circumferential and axial directions (figure 6) suggests that this overall model is best suited for smooth, continuous breaking. The poorer quality of the curve fits in the axial direction can be partially attributed to the fragmented and discontinuous curve profile, which is likely because of pulling against the main fibre orientation [45]. Similar effects have been observed in other failure tests such as peel testing [59].

However, an additional reason stems from the nature of the GOH model at high stretches. The GOH parameters that gave the best fit to the non-damage portion of the axial experimental curve, produce very large stress at the failure stretch. If the stress from the GOH model at the failure stretch was too high, the damage model could not reduce this stress sufficiently to produce a good fit to the experimental data. By adjusting the fitting procedure to reduce the gradient of the elastic portion of the curves, this large stress was reduced and the overall fit to the experimental data improved. This is reflected in all of the model curves for axial direction specimens: the model underestimates the stress until relatively close to the failure point, when it briefly switches to overestimation. The effects of this modification to the fitting of the GOH parameters can be seen when comparing figure 7 to the fitted GOH parameters in table 4a. Despite the very similar curve profile in the control and elastase treated samples, the fitted GOH parameters are very different. This is because there are multiple suitable candidate solutions for the circumferential direction that will yield equally good overall $r^2$ values to those seen here; that is, the model over fits the data. Fitting to the axial direction simultaneously reduced the number of candidate solutions and produced parameters that better represented the *overall* tissue behaviour. On the other hand, modifying the fitting procedure to achieve a better fit in the axial direction may also diminish the physical insight that can be derived from the resulting parameter values.

*4.2.2. GOH Parameters $k_1$ and $k_2$*

The $k_1$ parameter is lowest for collagenase data, which fits with the loss of collagen due to collagenase digestion. Additionally, elastase treated samples produced a higher $k_1$ than did the control samples, supporting the suggestion made previously that partial elastin digestion leads to collagen fibres altering their behaviour to compensate for the elastin loss. However, glutaraldehyde treated samples yielded the highest $k_1$, which may have resulted from the cross linking of collagen fibres making them stiffer. Interestingly, both elastase and collagenase produced small $k_2$ values, and since these both have statistically significant changes in fracture stretch in both directions, it implies a lower $k_2$ leads to a more gradual increase in stress with increasing stretch. Physiologically, this may reflect the collagen fibres requiring higher stretches to fully unravel.

The results agree to varying degrees with those in previous studies. Control samples produced similar $k_1$ values to those reported by Weisbecker, et al., but lower $k_2$ values [33]. Gundiah, et al. reported decreases in $k_2$ in collagenase samples compared with controls, as here, but with an accompanying increase in $k_1$, the latter not seen here [18]. Zeinali-Davarani, et al. performed gradual elastase digestion of porcine aorta [19]. They found that partial digestion led to a decrease in $k_2$ compared with control samples, as seen here. However, they also reported a decreased $k_1$ that we have not observed. Moreover, when nearly fully digested, both $k_1$ and $k_2$ were reported to increase sharply and to far higher values than found here.

*4.2.3. Fibre Angle $\theta$*

Fibre angle being lowest for collagenase samples could be a result of the collagenase altering the fibre attachment and alignment. This supports the theory in section 4.1.1 that collagen fibre recruitment in the axial direction has been hampered by this. Additionally, it is further supported by axial collagenase samples having the lowest overall fracture stress. lutaraldehyde samples having the highest $\theta$ implies a more isotropic response and could result from the increased density of cross links present in the tissue.

Comparing the control results to findings in the literature, $\theta$ is similar, which encourages confidence in the reliability of the fitted data [33]. However, histological and multiphoton microscopy investigations of collagen fibre orientation have suggested closer alignment with the circumferential direction than our model fits suggest. Polarised light microscopy has been utilised with human thoracic aorta and a mean fibre angle of approximately 27° was observed, far lower than our value [38]. Diffusion tensor imaging of porcine aorta further suggested an average alignment with the circumferential direction of 16° [60]. Electron and confocal microscopy performed on rat abdominal aorta similarly suggested strong mean alignment with the circumferential direction [61]. These discrepancies may reflect limitations of the GOH model itself (for example, with respect to its representation of the fibre mechanical response), or deficiencies in the fitting process after all.

Fibre angle for collagenase samples can be compared to the findings in Gundiah et al.: for controls and collagenase treated samples, $\theta$ was greater than found here, however the difference between the control and collagenase samples was similarly small: $< 4^o$ [18]. Zeinali-Davarani et al. reported an increase in $\theta$ compared to control samples for partial digestion, whereas a decrease is reported here [19]. However, they also found that $\theta$ reduces to a similar angle as the control with further digestion.

*4.2.4. Damage Parameters $\Xi^f_{\min}$ and $\Xi^f_{\max}$*

Damage in the axial direction was more gradual than in the circumferential direction and thus the same damage parameters could not be applied for both directions. This may be attributed to the interactions between fibre families differing in each loading direction. Therefore, fitting to both directions separately allowed these differences to be captured within the damage parameters and allowed the curve profiles to be matched closely enough for the parameters to have relevance. The is evident from the manually acquired $\Xi^f_{\min}$ and $\Xi^f_{\max}$ values: the spread was much larger in the axial than in the circumferential direction because the damage initiation could be discerned at much lower strain energies as a result of the more gradual breaking.

In the circumferential data, the more gradual collagenase failure may be used to justify the claims made in section 4.1 that the collagen fibre network may have been disrupted and thus the fibres will break more slowly. We might speculate that, with further digestion, the circumferential behaviour near failure will begin

to resemble that of the axial direction (beyond the inevitable loss of anisotropy); i.e., the failure will become more uneven with greater interruption to the collagen fibres.

*4.2.5. Diseased Tissue Comparison*

Two of the most prevalent and widely explored arterial diseases are atherosclerosis and aneurysm. He and Roach investigated the composition and mechanical properties of abdominal aortic aneurysms [62]. They stained the aortic wall to identify collagen fibres in histology and performed uniaxial tension tests in the axial direction. It was found that elastin and smooth muscle cell volume fraction decreased by approximately an order of magnitude compared with healthy tissue, whilst collagen volume fraction nearly doubled. Their tensile test data, correspondingly, showed increased stiffness in diseased tissue and curves shifted towards lower strains. This behaviour coincides with results reported in Gundiah et al. when elastin was artificially degraded [18]. However, it was not reflected in our results, wherein curves for elastase treated samples showed a shift towards higher strains. It could be speculated that to emulate the mechanical properties of aneurysm tissue, greater elastase digestion is necessary. Additionally, subsequent glutaraldehyde treatment may further emulate the increase in collagen volume, as the remaining collagen will be heavily cross-linked by this means.

Comparing failure behaviour, Raghavan et al. performed uniaxial tension tests on ruptured and unruptured human abdominal aorta aneurysms in the axial direction [63]. The mean failure stress for unruptured aneurysms ($0.95 \pm 0.28$ MPa) is similar to results reported here for all sample treatment types, but is closest to the values for glutaraldehyde and collagenase treated samples. However, the failure stretch in that study ($1.39 \pm 0.09$) is far lower than for all sample treatment types here. A possible explanation for this disparity is that the tissue investigated in that study is in the late stages of the aneurysm disease process. The treatments applied here were intended to partially degrade or cross-link collagen and elastin fibres, thus greater treatment time or concentration may allow the tissue to more closely emulate later stages of the aneurysm disease process, specifically.

One of the most complete investigation into changes in arterial wall mechanics in atherosclerosis was performed by Holzapfel et al. [64]. Here, uniaxial tension results from atherosclerotic intima and media from iliac arteries were compared with those of intima, media and adventitia from non-diseased sites. The results showed a pronounced difference in the media when stretched in the circumferential direction, with steeper curves and a higher ultimate tensile stress, despite the stretch at failure being much lower. In the axial direction the difference was far less clear and there seemed to be little difference between diseased and non-diseased media. The higher fracture stress in the circumferential direction coincides well with our results for elastase treated samples, however the lower fracture stretch does not. Closer approximation of this behaviour might be achieved with further elastase digestion or a combination of elastase digestion and glutaraldehyde treatment, as suggested previously.

Failure behaviour of atherosclerotic coronary artery was investigated in [65]. Axial and circumferential samples were stretched to failure and the failure stress and stretch were reported. The axial failure stress (Cauchy stress approximately $0.73 \pm 0.38$ MPa) was similar to the value reported in the present study for collagenase treated samples. Circumferential failure stress (Cauchy stress approximately $1.80 \pm 0.78$ MPa), while similarly closest to the present value for collagenase samples, was nonetheless substantially lower. Axial failure stretch was considerably smaller ($1.40 \pm 0.18$) than for any treated samples here. Circumferential failure stretch ($1.47 \pm 0.25$) was most like control, 20hC and glutaraldehyde sample values in this study but still much reduced. Longer treatment times may aid in reducing the circumferential fracture stress and fracture stretch in both directions. However, the true effects of the atherosclerotic plaques would likely *not* be confined to alterations in the elastin and collagen networks, and this could also explain the differences observed.

*4.3. Limitations*

As mentioned in the Introduction, disease processes are complex and multifaceted, and simple enzymatic digestion provides only an approximation of the various chemical, physical and cellular processes taking place within the arterial wall in processes such as aneurysm formation. Therein, for example, loss of elastin, and the accompanying increase in wall compliance, stimulates cellular mechanotransduction and, in turn,

complex remodelling of collagen components [66]. Wall mechanics in atherosclerosis are yet more complex due to the presence of the atherscleroticplaque which, despite efforts to capture its mechanical properties, is exceedingly difficult to incorporate into healthy arteries with many studies opting to induce the process *in vivo* [67, 68]. The physiological complexity of real disease processes notwithstanding, our aim in this work was to produce a physical model of diseased arteries that effectively emulates the accompanying changes in their mechanical properties only. However, as mentioned in section 4.2.5, judicious combination of any or all of these treatments could be used to effect the changes observed in a particular disease.

Mechanical testing in this study was performed at room temperature and in open air, whilst many other studies performed tensile tests within a saline bath. It has been previously mentioned in Section 2.1.2 that this was to allow for accurate recording of sample stretch. But methods similar to those employed by Loree et al. with a saline drip at 37°C may yield results with more physiological relevance [69].

Further physiological relevance could also be achieved with biaxial loading, which more closely reflects the *in vivo* loading conditions [70, 71, 72]. However, there are practical difficulties associated with using biaxial testing at high loads present in this study [73], and doing so may yield poor estimates of stress [74, 75]. Thus it is ill-suited to investigation of failure behaviour.

The GOH constitutive model was chosen due to its wide use for capturing arterial wall mechanics. In this work only the media response (assumed to be dominant) was investigated; the adventitia was removed and the intima thickness was small enough to be considered negligible. Despite using this relatively thin layer of tissue, a gradient of enzyme penetration must persist, meaning superficial regions will be more digested than interior ones. A constitutive model that incorporates different layers may accordingly enable the depth-dependence of mechanical properties that must accompany this gradient to be captured.

Additionally, while the GOH formulation has been shown to model well the tissue response in physiological strain ranges, the exponential fibre term may not be suitable outside this range, where it appears the collagen fibres transition from exponential to more linear behaviour [76]. A modified strain energy function that emulates the GOH response for moderate strains, but approaches linearity nearer to failure strains may thus be more widely applicable. Finally the applicability of the GOH model to arterial wall that has undergone enzymatic digestion has not been established; enzyme treatment may drastically alter fibre properties such that the underlying assumptions of the model may no longer be valid; and further investigation of this matter is required.

## 5. Conclusions

The goal of this study was to investigate the viability of enzyme degradation treatments as a means of producing physical models of diseased arteries. To this end, porcine arteries were treated with collagenase and elastase concentrations that allow for partial breakdown of constituent proteins to emulate the mechanical property changes that accompany disease. In addition, arteries were treated with a weak glutaraldehyde solution to induce minor cross-linking, similar to that seen in some in arterial diseases. Collagenase treated samples did not show significantly different fracture stresses from controls in the circumferential direction, but in the axial direction the difference was significant. Conversely, elastase samples showed a significant increase in fracture stress in the circumferential direction, but no significant difference in the axial direction. glutaraldehyde samples showed no significant difference in either direction. Axial direction curve profiles were, however, significantly changed by this treatment, showing more fragmented behaviour and damage initiating sooner.

To draw out quantitative comparisons to the curve profiles the commonly utilised GOH model was combined with a continuum damage model and fit to the experimental data. Both enzymatic treatments had a strong effect on fibre-related model terms, but only collagenase results suggested a strong change in fibre orientation. This model was best suited to circumferential data due to the smoother transition from damage initiation to complete failure.

Finally, given the variety of changes in different diseases (see description in the Introduction and comparison in section 4.2.5), the treatments described here appear indeed to provide a basis for creation of physical

models of diseased arteries, though further refinement of the treatment protocols may further improve the correspondence.

## 6. Acknowledgements

This work was supported by the European Commission Framework Programme 7, Understanding Interactions of Human Tissue with Medical Devices (UNITISS, FP7-PEOPLE-2011-IAPP/286174).

## 7. References

[1] B. Calvo, E. Pena, An uncoupled directional damage model for fibred biological soft tissues. formulation and computational aspects, International Journal for Numerical Methods in Engineering 69 (August 2006) (2007) 2036–2057. doi:10.1002/nme.

[2] T. C. Gasser, R. W. Ogden, G. A. Holzapfel, Hyperelastic modelling of arterial layers with distributed collagen fibre orientations., Journal of the Royal Society, Interface / the Royal Society 3 (6) (2006) 15–35. doi:10.1098/rsif.2005.0073.

[3] P. Bhatnagar, K. Wickramasinghe, J. Williams, M. Rayner, N. Townsend, The epidemiology of cardiovascular disease in the uk 2014, Heart 101 (15) (2015) 1182–1189. doi:10.1136/heartjnl-2015-307516.

[4] C. J. Van Andel, P. V. Pistecky, C. Borst, Mechanical properties of porcine and human arteries: Implications for coronary anastomotic connectors, Annals of Thoracic Surgery 76 (03) (2003) 58–64. doi:10.1016/S0003-4975(03)00263-7.

[5] A. V. Kamenskiy, I. I. Pipinos, Y. A. Dzenis, N. Y. Phillips, A. S. Desyatova, J. Kitson, R. Bowen, J. N. MacTaggart, Effects of age on the physiological and mechanical characteristics of human femoropopliteal arteries., Acta Biomaterialia 11 (2015) 304–13. doi:10.1016/j.actbio.2014.09.050.

[6] S. Glagov, R. Vito, D. P. Giddens, C. K. Zarins, Micro-architecture and composition of artery walls: relationship to location, diameter and the distribution of mechanical stress., Journal of Hypertension. 10 (6) (1992) 101–4. doi:10.1097/00004872-199208001-00026.

[7] T. Boulesteix, A.-M. Pena, N. Pagès, G. Godeau, M.-P. Sauviat, E. Beaurepaire, M.-C. Schanne-Klein, Micrometer scale ex vivo multiphoton imaging of unstained arterial wall structure, Cytometry Part A 69A (1) (2006) 20–26. doi:10.1002/cyto.a.20196.

[8] D. M. Basalyga, D. T. Simionescu, W. Xiong, B. T. Baxter, B. C. Starcher, N. R. Vyavahare, Elastin degradation and calcification in an abdominal aorta injury model: role of matrix metalloproteinases., Circulation 110 (22) (2004) 3480–7. doi:10.1161/01.CIR.0000148367.08413.E9.

[9] S. E. Greenwald, Ageing of the conduit arteries., The Journal of Pathology 211 (2) (2007) 157–72. doi:10.1002/path.2101.

[10] A. Y. Lee, B. Han, S. D. Lamm, C. A. Fierro, H.-C. Han, Effects of elastin degradation and surrounding matrix support on artery stability., American Journal of Physiology. Heart and Circulatory Physiology 302 (4) (2012) 873–84. doi:10.1152/ajpheart.00463.2011.

[11] M. J. Sherratt, Tissue elasticity and the ageing elastic fibre., Age 31 (4) (2009) 305–25. doi:10.1007/s11357-009-9103-6.

[12] A. Daugherty, L. a. Cassis, Mouse models of abdominal aortic aneurysms., Arteriosclerosis, Thrombosis, and Vascular Biology 24 (3) (2004) 429–34. doi:10.1161/01.ATV.0000118013.72016.ea.

[13] J. Ferruzzi, D. A. Vorp, J. D. Humphrey, On constitutive descriptors of the biaxial mechanical behaviour of human abdominal aorta and aneurysms., Journal of the Royal Society, Interface / the Royal Society 8 (56) (2011) 435–450. doi:10.1098/rsif.2010.0299.

[14] M. J. Barnes, Collagens in atherosclerosis, Collagen and Related Research 5 (1) (1985) 65–97. doi:10.1016/S0174-173X(85)80048-0.

[15] H. Lijnen, Extracellular proteolysis in the development and progression of atherosclerosis., Biochemical Society Transactions (2002) 63–67doi:10.1042/ [doi].

[16] Y. Seyama, H. Wachi, Atherosclerosis and matrix dystrophy., Journal of Atherosclerosis and Thrombosis 11 (5) (2004) 236–245. doi:10.5551/jat.11.236.

[17] C. M. Kielty, Elastic fibres in health and disease., Expert Reviews in Molecular Medicine 8 (19) (2006) 1–23. doi:10.1017/S146239940600007X.

[18] N. Gundiah, A. R. Babu, L. A. Pruitt, Effects of elastase and collagenase on the nonlinearity and anisotropy of porcine aorta., Physiological Measurement 34 (12) (2013) 1657–73. doi:10.1088/0967-3334/34/12/1657.

[19] S. Zeinali-Davarani, M.-J. Chow, R. Turcotte, Y. Zhang, Characterization of biaxial mechanical behavior of porcine aorta under gradual elastin degradation., Annals of Biomedical Engineering 41 (7) (2013) 1528–38. doi:10.1007/s10439-012-0733-y.

[20] A. J. Schriefl, T. Schmidt, D. Balzani, G. Sommer, G. A. Holzapfel, Selective enzymatic removal of elastin and collagen from human abdominal aortas: Uniaxial mechanical response and constitutive modeling, Acta Biomaterialia 17 (2015) 125–136. doi:10.1016/j.actbio.2015.01.003.

[21] E. Fonck, G. Prod'hom, S. Roy, L. Augsburger, D. A. Rüfenacht, N. Stergiopulos, Effect of elastin degradation on carotid wall mechanics as assessed by a constituent-based biomechanical model., American Journal of Physiology. Heart and Circulatory Physiology 292 (6) (2007) 2754–63. doi:10.1152/ajpheart.01108.2006.

[22] P. Kochová, J. Kuncová, J. Svíglerová, R. Cimrman, M. Miklíková, V. Liška, Z. Tonar, The contribution of vascular smooth muscle, elastin and collagen on the passive mechanics of porcine carotid arteries., Physiological Measurement 33 (8) (2012) 1335–51. doi:10.1088/0967-3334/33/8/1335.

[23] H.-Y. Lee, B.-H. Oh, Aging and arterial stiffness, Circulation Journal 74 (11) (2010) 2257–2262. doi:10.1253/circj.CJ-10-0910.

[24] R. Martinez, H.-C. Han, The effect of collagenase on the critical buckling pressure of arteries., Molecular & Cellular Biomechanics 9 (1) (2012) 55–75.

[25] L. Dadgar, Y. Marois, X. Deng, R. Guidoin, Arterial wall mechanical characteristics after treatment in collagenase: An in vitro aneurysm model, Clinical and Investigative Medicine 20 (1) (1997) 25–34.

[26] P. F. Gratzer, J. M. Lee, Altered mechanical properties in aortic elastic tissue using glutaraldehyde/solvent solutions of various dielectric constant., Journal of Biomedical Materials Research 37 (4) (1997) 497–507.

[27] M. Sawabe, Vascular aging: from molecular mechanism to clinical significance., Geriatrics and Gerontology International 10 Suppl 1 (2010) 213–20. doi:10.1111/j.1447-0594.2010.00603.x.

[28] V. Alastrué, J. Rodríguez, B. Calvo, M. Doblaré, Structural damage models for fibrous biological soft tissues, International Journal of Solids and Structures 44 (18-19) (2007) 5894–5911. doi:10.1016/j.ijsolstr.2007.02.004.

[29] G. A. Holzapfel, Determination of material models for arterial walls from uniaxial extension tests and histological structure., Journal of Theoretical Biology 238 (2) (2006) 290–302. doi:10.1016/j.jtbi.2005.05.006.

[30] M. T. Walsh, E. M. Cunnane, J. J. Mulvihill, A. C. Akyildiz, F. J. H. Gijsen, G. A. Holzapfel, Uniaxial tensile testing approaches for characterisation of atherosclerotic plaques, Journal of Biomechanics 47 (4) (2014) 793–804. doi:10.1016/j.jbiomech.2014.01.017.

[31] R. H. Cox, Passive mechanics and connective tissue composition of canine arteries., The American Journal of Physiology 234 (5) (1978) H533–H541.

[32] G. A. Holzapfel, T. C. Gasser, R. W. Ogden, A new constitutive framework for arterial wall mechanics and a comperative study of material models, Journal of Elasticity 61 (2000) 1–48. doi:10.1023/A:1010835316564.

[33] H. Weisbecker, D. M. Pierce, P. Regitnig, G. A. Holzapfel, Layer-specific damage experiments and modeling of human thoracic and abdominal aortas with non-atherosclerotic intimal thickening., Journal of the Mechanical Behavior of Biomedical Materials 12 (2012) 93–106. doi:10.1016/j.jmbbm.2012.03.012.

[34] H. Weisbecker, C. Viertler, D. M. Pierce, G. A. Holzapfel, The role of elastin and collagen in the softening behavior of the human thoracic aortic media., Journal of Biomechanics 46 (11) (2013) 1859–65. doi:10.1016/j.jbiomech.2013.04.025.

[35] G. A. Holzapfel, Nonlinear solid mechanics: a continuum approach for engineering, Vol. 24, John Wiley & Sons, Ltd., 2000.

[36] J. Simo, On a fully three-dimensional finite-strain viscoelastic damage model: Formulation and computational aspects, Computer Methods in Applied Mechanics and Engineering 60 (2) (1987) 153–173. doi:10.1016/0045-7825(87)90107-1.

[37] E. Peña, B. Calvo, M. A. Martínez, M. Doblaré, On finite-strain damage of viscoelastic-fibred materials. application to soft biological tissues, International Journal for Numerical Methods in Engineering 74 (7) (2008) 1198–1218. doi:10.1002/nme.2212.

[38] A. J. Schriefl, G. Zeindlinger, D. M. Pierce, P. Regitnig, G. A. Holzapfel, Determination of the layer-specific distributed collagen fibre orientations in human thoracic and abdominal aortas and common iliac arteries, Journal of the Royal Society, Interface / the Royal Society 12 (December 2011) (2012) 1275–1286.

[39] D. Robertson, D. Cook, Unrealistic statistics: How average constitutive coefficients can produce non-physical results, Journal of the Mechanical Behavior of Biomedical Materials 40 (2014) 234–239. doi:10.1016/j.jmbbm.2014.09.006.

[40] J. Kennedy, R. Eberhart, Particle swarm optimization, Neural Networks, 1995. Proceedings., IEEE International Conference on 4 (1995) 1942–1948. doi:10.1109/ICNN.1995.488968.

[41] R. W. Ogden, G. Saccomandi, I. Sgura, Fitting hyperelastic models to experimental data, Computational Mechanics 34 (6) (2004) 484–502. doi:10.1007/s00466-004-0593-y.

[42] G. A. Holzapfel, R. W. Ogden, Constitutive modelling of arteries, Proceedings of the Royal Society A: Mathematical, Physical and Engineering Sciences 466 (2118) (2010) 1551–1597. doi:10.1098/rspa.2010.0058.

[43] Y. C. Fung, K. Fronek, P. Patitucci, Pseudoelasticity of arteries and the choice of its mathematical expression., The American Journal of Physiology 237 (5) (1979) H620–H631.

[44] B. D. Stemper, N. Yoganandan, M. R. Stineman, T. A. Gennarelli, J. L. Baisden, F. a. Pintar, Mechanics of fresh, refrigerated, and frozen arterial tissue, Journal of Surgical Research 139 (2) (2007) 236–242. doi:10.1016/j.jss.2006.09.001.

[45] B. D. Stemper, N. Yoganandan, F. A. Pintar, Mechanics of arterial subfailure with increasing loading rate, Journal of Biomechanics 40 (8) (2007) 1806–1812. doi:10.1016/j.jbiomech.2006.07.005.

[46] D. Mohan, J. W. Melvin, Failure properties of passive human aortic tissue. i–uniaxial tension tests., Journal of Biomechanics 15 (11) (1982) 887–902. doi:10.1016/0021-9290(83)90044-1.

[47] R. Collins, W. C. Hu, Dynamic deformation experiments on aortic tissue., Journal of Biomechanics 5 (4) (1972) 333–337. doi:10.1016/0021-9290(72)90062-0.

[48] H. D. Intengan, G. Thibault, J. S. Li, E. L. Schiffrin, Resistance artery mechanics, structure, and extracellular components in spontaneously hypertensive rats : effects of angiotensin receptor antagonism and converting enzyme inhibition., Circulation 100 (22) (1999) 2267–2275. doi:10.1161/01.CIR.100.22.2267.

[49] P. B. Dobrin, T. R. Canfield, Elastase, collagenase, and the biaxial elastic properties of dog carotid artery., The American Journal of Physiology 247 (1 Pt 2) (1984) H124–H131.

[50] P. B. Dobrin, W. C. Gley, Elastase, collagenase and the radial elastic properties of arteries., Experientia 41 (8) (1985) 1040–1042. doi:10.1007/BF01952132.

[51] M. J. Collins, J. F. Eberth, E. Wilson, J. D. Humphrey, Acute mechanical effects of elastase on the infrarenal mouse aorta: implications for models of aneurysms., Journal of Biomechanics 45 (4) (2012) 660–5. doi:10.1016/j.jbiomech.2011.12.013.

[52] M.-J. Chow, J. R. Mondonedo, V. M. Johnson, Y. Zhang, Progressive structural and biomechanical changes in elastin degraded aorta., Biomechanics and Modeling in Mechanobiology 12 (2) (2013) 361–72. doi:10.1007/s10237-012-0404-9.

[53] P. Lacolley, P. Boutouyrie, M. Glukhova, J.-M. Daniel Lamaziere, P.-F. Plouin, P. Bruneval, P. Vuong, P. Corvol, S. Laurent, Disruption of the elastin gene in adult williams syndrome is accompanied by a paradoxical reduction in arterial stiffness., Clinical Science 103 (1) (2002) 21–29. doi:10.1042/CS20010287.

[54] S. Avrameas, Coupling of enzymes to proteins with glutaraldehyde. use of the conjugates for the detection of antigens and antibodies., Immunochemistry 6 (1) (1969) 43–52. doi:10.1016/0019-2791(69)90177-3.

[55] S. Avrameas, T. Ternynck, The cross-linking of proteins with glutaraldehyde and its use for the preparation of immunoadsorbents., Immunochemistry 6 (1) (1969) 53–66. doi:10.1016/0019-2791(69)90178-5.

[56] E. M. McDowell, B. F. Trump, Histologic fixatives suitable for diagnostic light and electron microscopy., Archives of Pathology & Laboratory Medicine 100 (8) (1976) 405–414.

[57] G. J. L'Italien, J. Megerman, J. E. Hasson, A. E. Meyer, R. E. Baier, W. M. Abbott, Compliance changes in glutaraldehyde-treated arteries., The Journal of Surgical Research 41 (2) (1986) 182–188. doi:10.1016/0022-4804(86)90023-5.

[58] H. W. Sung, C. S. Hsu, Y. S. Lee, Physical properties of a porcine internal thoracic artery fixed with an epoxy compound, Biomaterials 17 (24) (1996) 2357–2365. doi:10.1016/S0142-9612(96)00081-6.

[59] G. Sommer, T. C. Gasser, P. Regitnig, M. Auer, G. A. Holzapfel, Dissection properties of the human aortic media: an experimental study., Journal of Biomechanical Engineering 130 (2) (2008) 021007. doi:10.1115/1.2898733.

[60] V. Flamini, C. Kerskens, C. Simms, C. Lally, Fibre orientation of fresh and frozen porcine aorta determined non-invasively using diffusion tensor imaging, Medical Engineering & Physics 35 (6) (2013) 765–776. doi:10.1016/j.medengphy.2012.08.008.

[61] M. K. O'Connell, S. Murthy, S. Phan, C. Xu, J. Buchanan, R. Spilker, R. L. Dalman, C. K. Zarins, W. Denk, C. A. Taylor, The three-dimensional micro- and nanostructure of the aortic medial lamellar unit measured using 3d confocal and electron microscopy imaging., Matrix Biology 27 (3) (2008) 171–81. doi:10.1016/j.matbio.2007.10.008.

[62] C. M. He, M. R. Roach, The composition and mechanical properties of abdominal aortic aneurysms, Journal of Vascular Surgery 20 (1) (1994) 6–13. doi:10.1016/0741-5214(94)90169-4.

[63] M. L. Raghavan, M. M. Hanaoka, J. A. Kratzberg, M. de Lourdes Higuchi, E. S. da Silva, Biomechanical failure properties and microstructural content of ruptured and unruptured abdominal aortic aneurysms., Journal of Biomechanics 44 (13) (2011) 2501–7. doi:10.1016/j.jbiomech.2011.06.004.

[64] G. A. Holzapfel, G. Sommer, P. Regitnig, Anisotropic mechanical properties of tissue components in human atherosclerotic plaques., Journal of Biomechanical Engineering 126 (5) (2004) 657–665. doi:10.1115/1.1800557.

[65] Z. Teng, D. Tang, J. Zheng, P. K. Woodard, A. H. Hoffman, An experimental study on the ultimate strength of the adventitia and media of human atherosclerotic carotid arteries in circumferential and axial directions, Journal of Biomechanics 42 (15) (2009) 2535–2539. doi:10.1016/j.jbiomech.2009.07.009.

[66] J. C. Lasheras, The biomechanics of arterial aneurysms, Annual Review of Fluid Mechanics 39 (1) (2007) 293–319. doi:10.1146/annurev.fluid.39.050905.110128.

[67] K. Hayashi, Y. Imai, Tensile property of atheromatous plaque and an analysis of stress in atherosclerotic wall, Journal of Biomechanics 30 (6) (1997) 573–579. doi:10.1016/S0021-9290(96)00185-6.

[68] G. S. Getz, C. a. Reardon, Animal models of atherosclerosis, Arteriosclerosis, Thrombosis, and Vascular Biology 32 (5) (2012) 1104–1115. doi:10.1161/ATVBAHA.111.237693.Animal.

[69] H. M. Loree, A. J. Grodzinsky, S. Y. Park, L. J. Gibson, R. T. Lee, Static circumferential tangential modulus of human atherosclerotic tissue, Journal of Biomechanics 27 (2) (1994) 195–204. doi:10.1016/0021-9290(94)90209-7.

[70] M. S. Sacks, Biaxial mechanical evaluation of planar biological materials, Journal of Elasticity 61 (1-3) (2000) 199–246. doi:10.1023/A:1010917028671.

[71] J. D. Humphrey, Cardiovascular Solid Mechanics: Cells, Tissues, and Organs, Springer-Verlag, 2002.

[72] J. P. Vande Geest, M. S. Sacks, D. A. Vorp, Age dependency of the biaxial biomechanical behavior of human abdominal aorta., Journal of Biomechanical Engineering 126 (6) (2004) 815–822. doi:10.1115/1.1824121.

[73] J. A. Peña, M. A. Martínez, E. Peña, Layer-specific residual deformations and uniaxial and biaxial mechanical properties of thoracic porcine aorta, Journal of the Mechanical Behavior of Biomedical Materials 50 (2015) 55–69. doi:10.1016/j.jmbbm.2015.05.024.

[74] W. Sun, M. S. Sacks, M. J. Scott, Effects of boundary conditions on the estimation of the planar biaxial mechanical properties of soft tissues., Journal of biomechanical engineering 127 (4) (2005) 709–715. doi:10.1115/1.1933931.

[75] S. D. Waldman, J. Michael Lee, Boundary conditions during biaxial testing of planar connective tissues. part 1: Dynamic behavior, Journal of Materials Science: Materials in Medicine 13 (10) (2002) 933–938. doi:10.1023/A:1019896210320.

[76] E. A. Stephen, A. Venkatasubramaniam, T. A. Good, L. D. T. Topoleski, The effect of glycation on arterial microstructure and mechanical response., Journal of Biomedical Materials Research. Part A 102 (8) (2014) 2565–72. doi:10.1002/jbm.a.34927.

**Appendix A: Cauchy stress derivation**

To evaluate $\sigma_1$, p must be eliminated from (5) using known constraints. First, $\lambda_1^{-1}\lambda_2^{-1} = \lambda_3$ if we assume incompressibility. Then, we further assume the collagen fibres have no component in the radial direction so $a_{i3} = 0$. First and fourth invariants of $\mathbf{C}$ and $\mathbf{a}_i \otimes \mathbf{a}_i$ may then be defined as $I_1 = \lambda_1^2 + \lambda_2^2 + \lambda_1^{-2}\lambda_2^{-2}$ and $I_{i4} = a_{i1}^2\lambda_1^2 + a_{i2}^2\lambda_2^2$.

Using these definitions, equation (4) may be rewritten as $E_i = \kappa I_1 + (1 - 3\kappa)I_{i4} - 1$, which yields an expression in terms of the principal stretches:

$$E_i = \kappa(\lambda_1^2 + \lambda_2^2 + \lambda_1^{-2}\lambda_2^{-2}) + (1 - 3\kappa)(a_{i1}^2\lambda_1^2 + a_{i2}^2\lambda_2^2), \quad i = 1, 2$$

allowing the derivative of (5) to be evaluated for $\Psi_i^f$ and $\Psi^m$. In uniaxial extension in the 1-direction, we will have $\sigma_2 = 0$, allowing $p$ to be obtained from (2.5) as:

$$p = \sigma_2 = \lambda_2 \frac{\partial \Psi(\lambda_1, \lambda_2, \mathbf{a}_1, \mathbf{a}_2)}{\partial \lambda_2}.$$

The required first principal stress then becomes:

$$\sigma_1 = \lambda_1 \frac{\partial \Psi(\lambda_1, \lambda_2, \mathbf{a}_1, \mathbf{a}_2)}{\partial \lambda_1} - \lambda_2 \frac{\partial \Psi(\lambda_1, \lambda_2, \mathbf{a}_1, \mathbf{a}_2)}{\partial \lambda_2},$$

wherein the required derivatives are easily evaluated.

## Tables and Figures

| Treatment | Solution | Temp. | Duration | N(axial) | N(circ) |
|---|---|---|---|---|---|
| Control (Fresh) | - | - | Fresh | 16 | 16 |
| 20 hour Control (20hC) | - | 37°C | 20 hours | 10 | 14 |
| Collagenase (Roche) | 0.05 U/ml | 37°C | 20 hours | 10 | 11 |
| Elastase (Sigma Aldrich) | 0.2 U/ml | 37°C | 20 hours | 13 | 11 |
| Glutaraldehyde | 0.1% | 4°C | 20 hours | 14 | 14 |

Table 1: Enzyme, glutaraldehyde and control treatment concentrations and durations.

| Elastic (GOH) parameters | Damage parameter |
|---|---|
| $k_1$ | $\beta^f$ |
| $k_2$ | |
| $\theta$ | |

Table 2: The constitutive parameters being found during each optimisation. $\theta$ is the collagen fibre angle.

| Fracture Stress (MPa) | | | | |
|---|---|---|---|---|
| Control | Control 20 hours | Collagenase | Elastase | Glutaraldehyde |
| 1.3 ± 0.41 | 1.33 ± 0.45 | 0.79 ± 0.37 | 1.48 ± 0.72 | 1.17 ± 0.477 |
| - | n.s. | $p<0.05$ | n.s. | n.s. |
| Stretch in 1st Principal Direction at Fracture | | | | |
| Control | Control 20 hours | Collagenase | Elastase | Glutaraldehyde |
| 1.84 ± 0.18 | 1.83 ± 0.24 | 2.10 ± 0.26 | 2.09 ± 0.29 | 1.77 ± 0.29 |
| - | n.s. | $p<0.05$ | $p<0.05$ | n.s. |

(a) Axial specimens.

| Fracture Stress (MPa) | | | | |
|---|---|---|---|---|
| Control | Control 20 hours | Collagenase | Elastase | Glutaraldehyde |
| 2.7 ± 0.61 | 2.96 ± 0.68 | 2.36 ± 1.01 | 4.35 ± 1.03 | 2.95 ± 0.74 |
| - | n.s. | n.s. | $p<0.05$ | n.s. |
| Stretch in 1st Principal Direction at Fracture | | | | |
| Control | Control 20 hours | Collagenase | Elastase | Glutaraldehyde |
| 1.6 ± 0.09 | 1.62 ± 0.09 | 1.73 ± 0.16 | 1.72 ± 0.09 | 1.63 ± 0.10 |
| - | n.s. | $p<0.05$ | $p<0.05$ | n.s. |

(b) Circumferential specimens.

Table 3: Fracture stress and stretch values (mean ± standard deviation), and results of student's unpaired $t$-test between control and treated samples. Data shown for fresh porcine aorta samples (control), samples incubated in saline solution at 37° C for 20 hours (20 hour control), collagenase treated samples, elastase treated samples and glutaraldehyde treated samples.

| **Sample** | $k_1$(kPa) | $k_2$ | $\theta$ (Degrees) |
|---|---|---|---|
| Control | 143 | 4.45 | 40.8 |
| Collagenase | 66.0 | 2.23 | 37.3 |
| Elastase | 222 | 1.77 | 38.7 |
| Glutaraldehyde | 283 | 2.54 | 41.1 |

(a) Fitted Gasser Ogden Holzapfel model parameters.

| | Axial | | | Circumferential | | |
|---|---|---|---|---|---|---|
| **Sample** | $\Xi^f_{\min}$ | $\Xi^f_{\max}$ | $\beta^f$ | $\Xi^f_{\min}$ | $\Xi^f_{\max}$ | $\beta^f$ |
| Control | 233 | 897 | 0.84 | 585 | 659 | 0.08 |
| Collagenase | 229 | 599 | -0.03 | 530 | 823 | 0.71 |
| Elastase | 351 | 970 | 0.70 | 835 | 944 | -0.75 |
| Glutaraldehyde | 296 | 995 | 0.82 | 680 | 797 | -1 |

(b) Damage parameters found by identification, alongside fitted $\beta_f$ parameter.

| **Sample** | $r^2$ axial | $r^2$ circumferential |
|---|---|---|
| Control | 0.85 | 1.00 |
| Collagenase | 0.90 | 0.99 |
| Elastase | 0.86 | 0.99 |
| Glutaraldehyde | 0.90 | 0.98 |

(c) Correlation coefficients ($r^2$) for the whole fitted curves compared to the experimental data.

Table 4: GOH and CDM parameters estimated from experimental data.

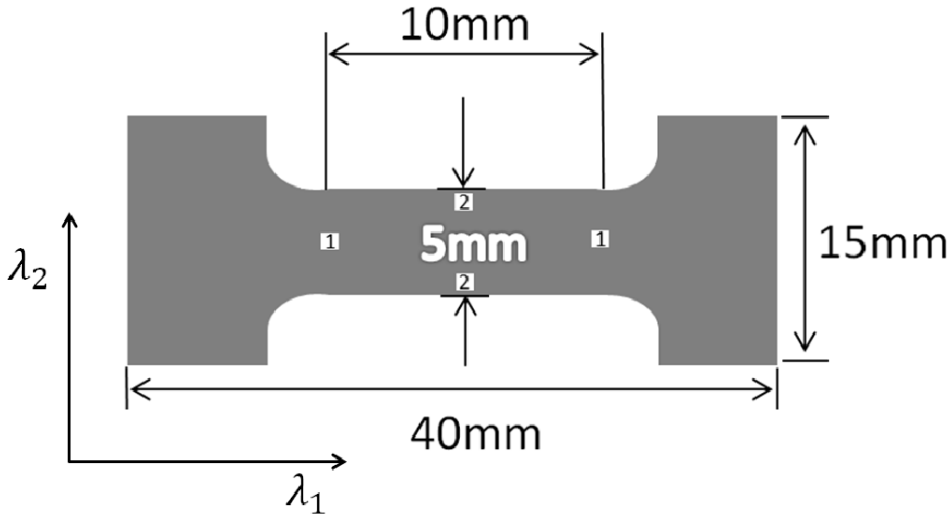


Figure 1: Sample geometry with marker positions indicated (white squares). Marker labels indicate the principal stretch direction characterised with that label.

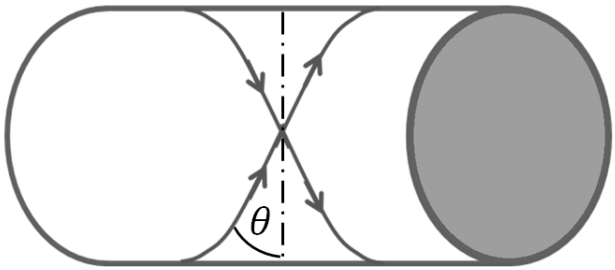


Figure 2: Representation of the mean collagen fibre angle $\theta$ in the GOH model. The model assumes that two collagen fibre families, with mean orientations indicated by the two arrowed lines, symmetrically encircle the blood vessel wall in a helicoidal manner. In this work, $\theta$ is defined with respect to the circumferential direction.

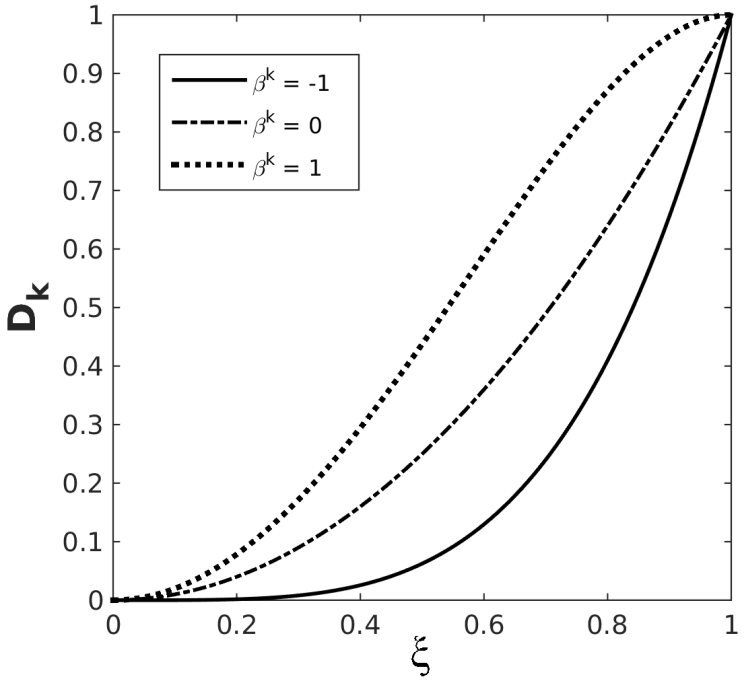


Figure 3: The relationship between $D^k$ and $\xi$ in (11) for $\beta^k = 1, 0$ and -1. $\xi = 0$ is the point of damage initiation and $\xi = 1$ is the point of complete failure of the material.

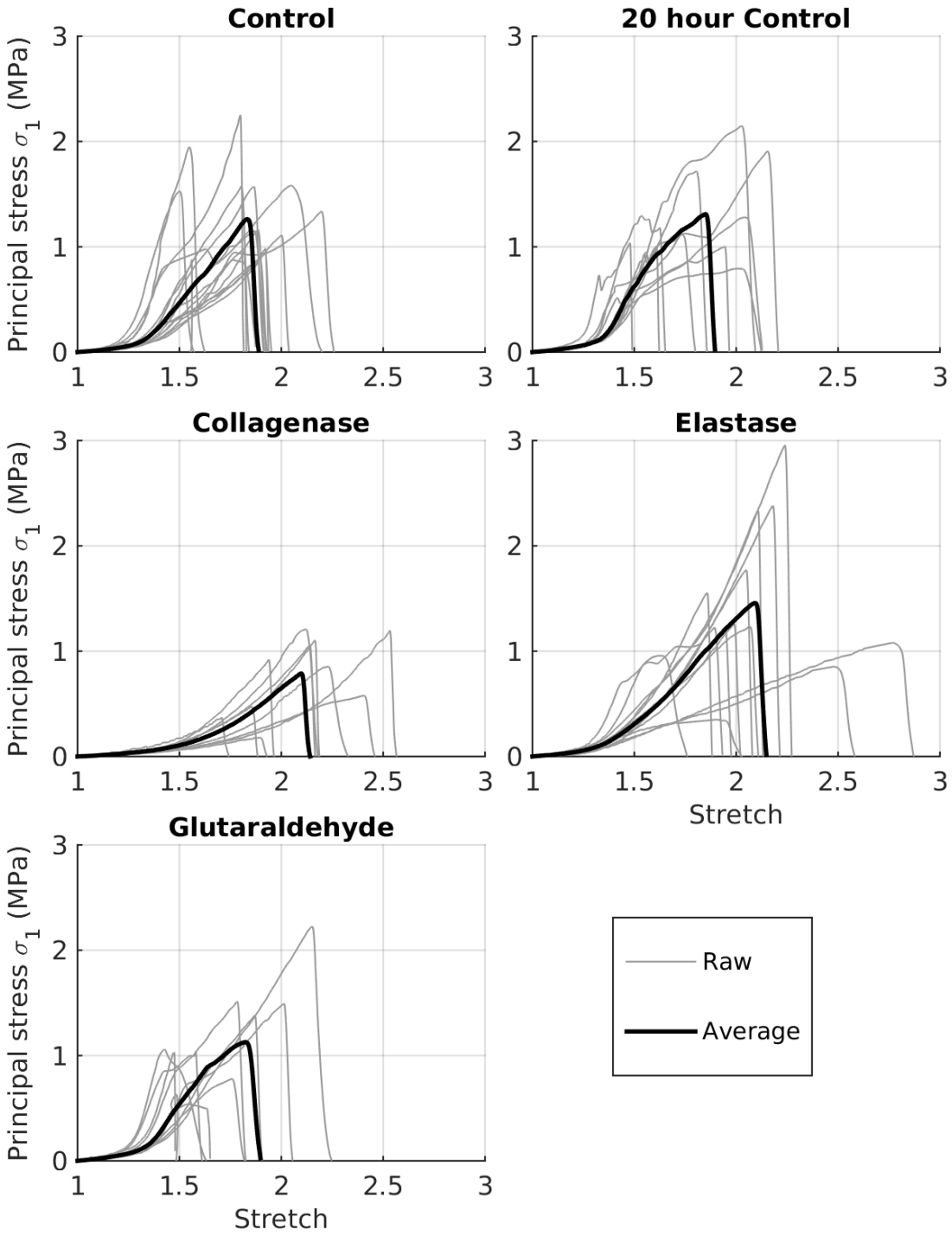


Figure 4: *Axial specimens.* First principal Cauchy stress versus stretch for the fresh porcine aorta samples (control), samples incubated in saline solution at 37° C for 20 hours (20 hour control), collagenase treated samples, elastase treated samples and glutaraldehyde treated samples. Raw experimental curves overlaid with averaged curves in all cases.

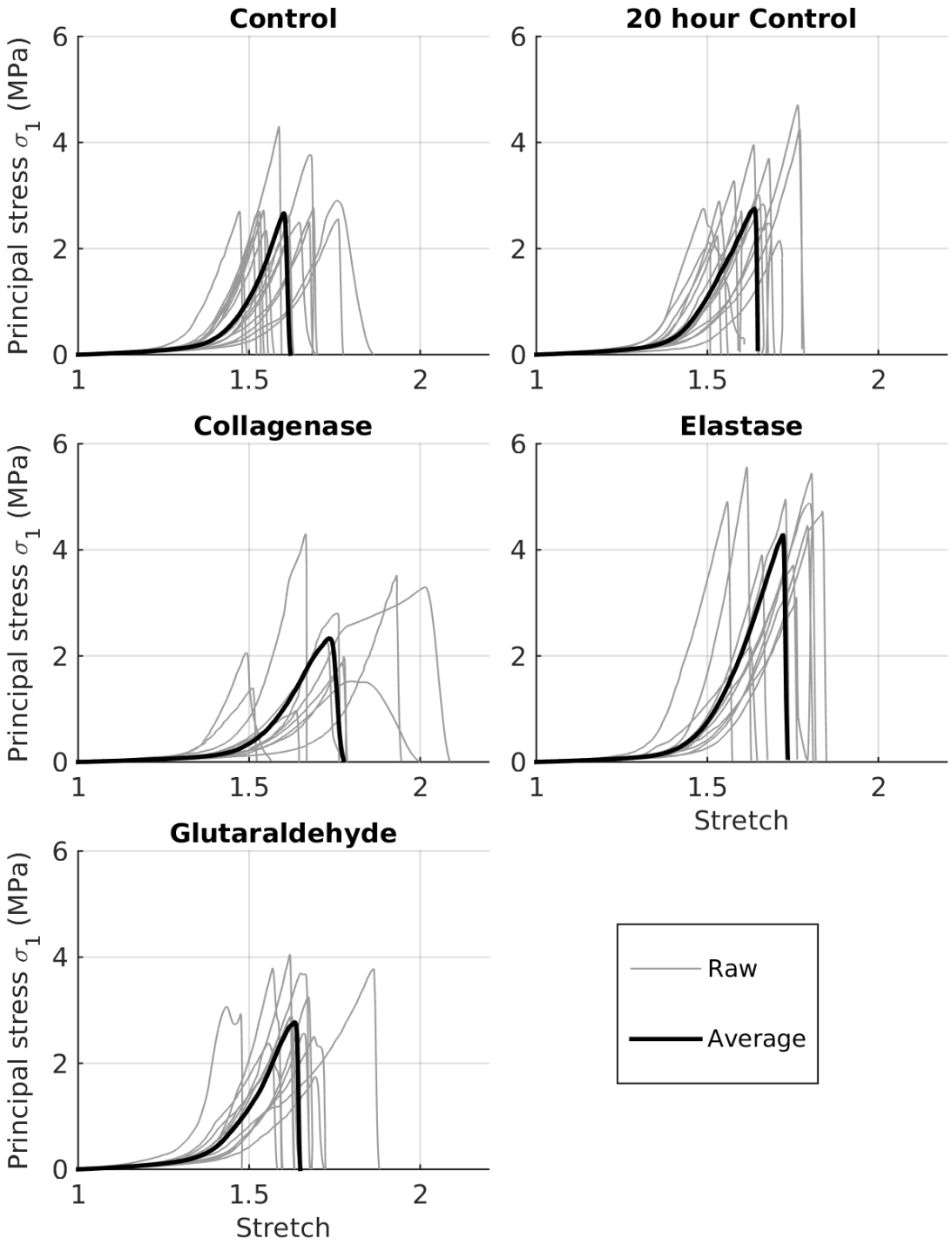


Figure 5: *Circumferential specimens.* First principal Cauchy stress versus stretch for the fresh porcine aorta samples (control), samples incubated in saline solution at 37° C for 20 hours (20 hour control), collagenase treated samples, elastase treated samples and glutaraldehyde treated samples. Raw experimental curves overlaid with averaged curves in all cases.

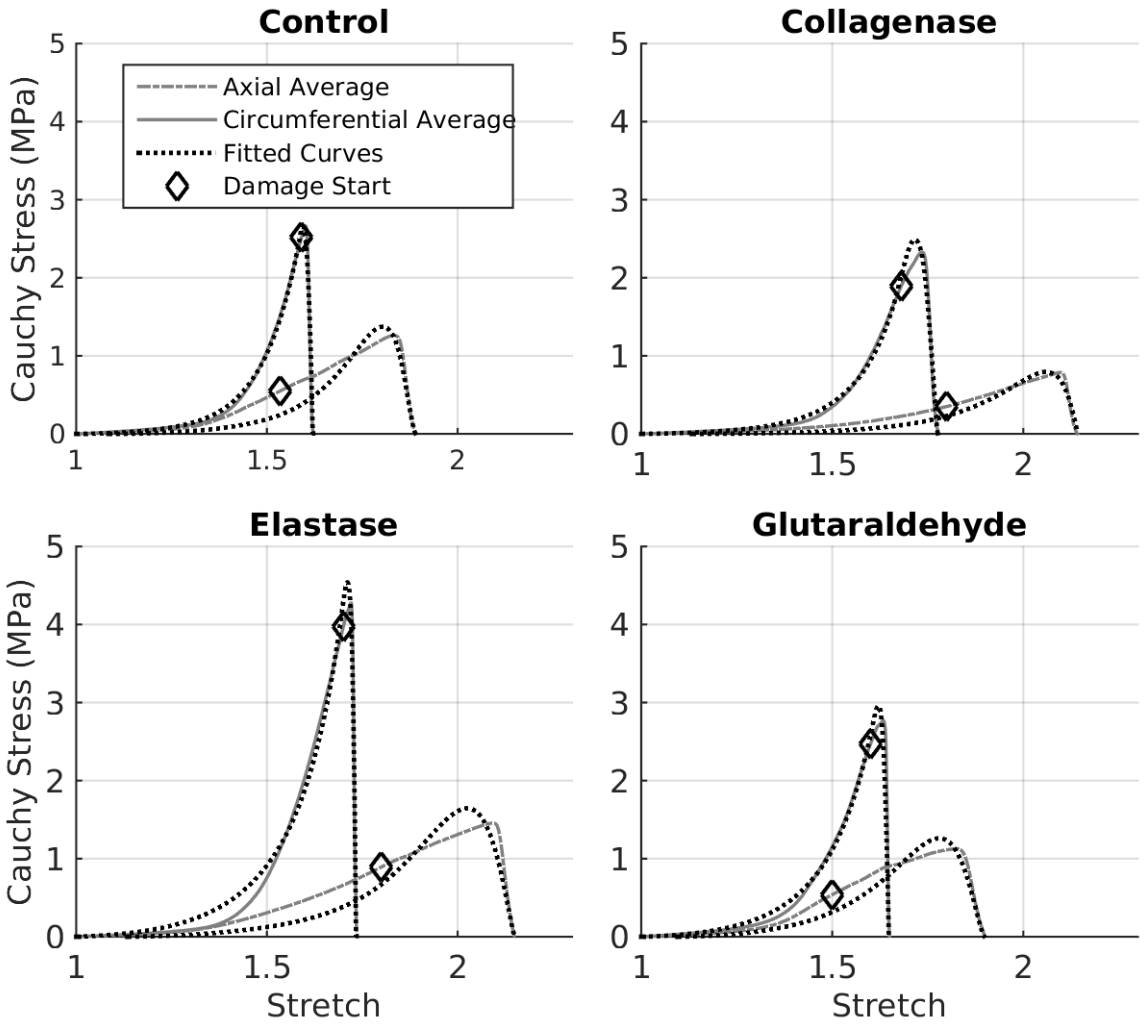


Figure 6: Average stretch versus Cauchy stress with curve fits overlaid. Diamonds mark the points at which damage was assumed to initiate. Non-damage parameters were fitted to the curve regions prior to these points.

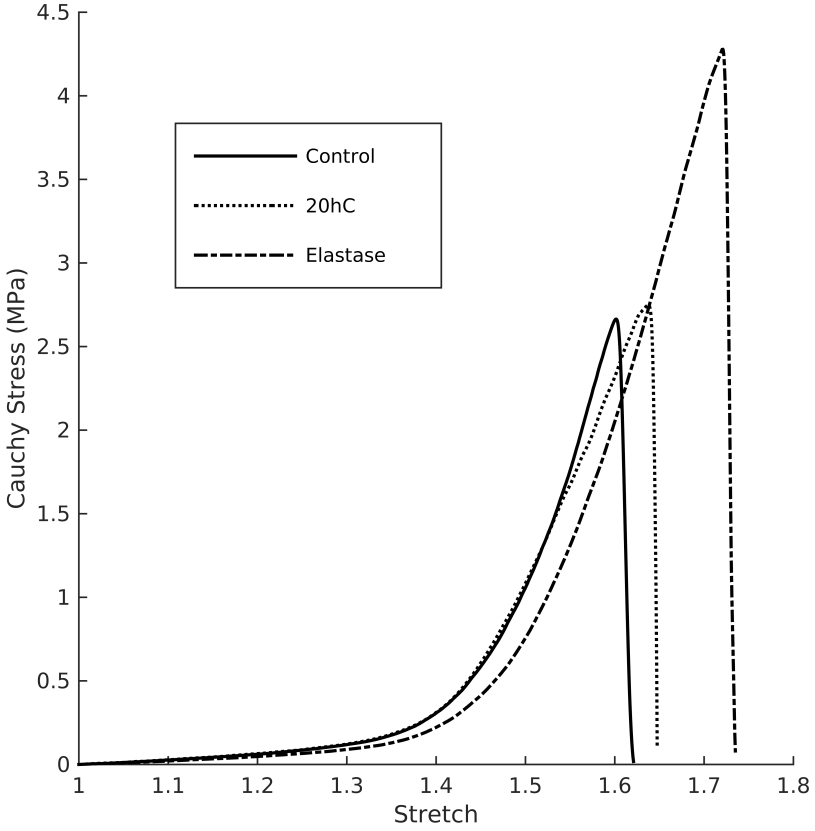


Figure 7: Direct comparison of control and 20hC average data with elastase average data in the circumferential direction.